Published in final edited form as:
J Magn Reson. 2015 October ; 259: 199–206. doi:10.1016/j.jmr.2015.08.018.

Correcting surface coil excitation inhomogeneities in single-shot SPatiotemporal ENcoding (SPEN) MRI

Rita Schmidt[#1], **Mor Mishkovsky**[#2], **Jean-Noel Hyacinthe**[3], **Nicolas Kunz**[4], **Rolf Gruetter**[2,4], **Arnaud Comment**[5], and **Lucio Frydman**[1]

[1]Department of Chemical Physics, Weizmann Institute of Science, Rehovot, Israel [2]Laboratory of Functional and Metabolic Imaging, Ecole Polytechnique Fédérale de Lausanne (EPFL), Lausanne, Switzerland [3]School of health, University of Applied Sciences and Arts Western Switzerland, Geneva, Switzerland [4]Center of Biomedical Imaging (CIBM), Ecole Polytechnique Fédérale de Lausanne (EPFL), Lausanne, Switzerland [5]Institute of the Physics of Biological Systems, Ecole Polytechnique Fédérale de Lausanne (EPFL), Lausanne, Switzerland

[#] These authors contributed equally to this work.

Abstract

Given their high sensitivity and ability to limit the field of view (FOV), surface coils are often used in magnetic resonance spectroscopy (MRS) and imaging (MRI). A major downside of surface coils is their inherent radiofrequency (RF) B_1 heterogeneity across the FOV, decreasing with increasing distance from the coil and giving rise to image distortions due to non-uniform spatial responses. A robust way to compensate for B_1 inhomogeneities is to employ adiabatic inversion pulses, yet these are not well adapted to all imaging sequences –including to single-shot approaches like echo planar imaging (EPI). Hybrid spatiotemporal encoding (SPEN) sequences relying on frequency-swept pulses provide another ultrafast MRI alternative, that could help solve this problem thanks to their built-in heterogeneous spatial manipulations. This study explores how this intrinsic SPEN-based spatial discrimination, could be used to compensate for the B_1 inhomogeneities inherent to surface coils. Experiments carried out in both phantoms and *in vivo* rat brains demonstrate that, by suitably modulating the amplitude of a SPEN chirp pulse that progressively excites the spins in a direction normal to the coil, it is possible to reduce RF transmit inhomogeneities and thus improve sensitivity and image fidelity.

Keywords

Ultrafast MRI; Spatiotemporal encoding; B_1 corrections; swept pulses; surface coil MRI

1 Introduction

Contemporary magnetic resonance imaging (MRI) offers a variety of contrast sources that extend well beyond the classical T_1 and T_2 image weightings. Physiological parameters such

Corresponding authors: Prof. Lucio Frydman; +972-8-9344903 lucio.frydman@weizmann.ac.il, Dr. Mor Mishkovsky +41 21 69 30590 mor.mishkovsky@epfl.ch.

Europe PMC Funders Author Manuscripts

as pH and temperature can be detected and mapped using chemical exchange saturation transfer (CEST);1,2 hyperpolarized MRI delivers real-time measurements of metabolic substrates and/or sensitized contrast agents;3–4 tissue oxygenation can be mapped in real-time functional studies via the BOLD effect;5 morphology and abnormalities can be revealed using diffusion weighted imaging (DWI)6 and diffusion tensor imaging (DTI) routines7. Although all these MRI approaches are different in nature and in their observables, they all share an important demand in common: they require ultrafast imaging protocols to record the *in vivo* physiological changes that they target. Various schemes have thus been proposed to reduce the time needed to acquire such MRI images. Some, like FLASH, RARE and their variants,8,9rely on rapid repetitions of single *k*-space line acquisitions; although highly robust, these often are not fast enough to deliver the kind of information mentioned above. Such experiments are thus often done using “ultrafast” sequences, specifically designed for acquiring the entire multidimensional *k*-space in a single scan.10 Foremost among these counts echo-planar imaging (EPI)11. Despite its video-rate ability EPI requires sampling its phase-encoded dimension with a relatively low effective bandwidth, leading to strong potential image distortions in inhomogeneous magnetic fields.

In recent years, hybrid spatiotemporal encoding (SPEN) schemes have been proposed as alternatives to overcome these single-scan MRI acquisition limitations.12,13 Originating in concepts related to the acquisition of multidimensional MRS data in a single-scan, SPEN’s low-bandwidth dimension is not bound by the Nyquist criteria that apply to EPI, and can thus provide higher immunities to B_0 inhomogeneities. Recent studies have shown these advantages with SPEN applications that included diffusion14, functional MRI15, perfusion imaging16 and chemical shift spectroscopic imaging17 studies. SPEN pulse sequences differ from their EPI counterparts in that, instead of relying on a single excitation pulse, they include linearly-swept “chirped” radiofrequency (RF) pulses applied in the presence of a magnetic field gradient. This results in a sequential excitation of the spins along the gradient’s direction, leading to a uniaxial quadratic phase profile, whose “stationary point” can be displaced throughout the sample by the application of an acquisition gradient. When coupled to a regular readout gradient oscillation this provides a way of rastering the low-bandwidth dimension of a 2D image acquisition without the constraints of a Fourier transform –directly in the image domain. This offers the opportunity to obtain high-fidelity images even in inhomogeneous B_o fields that would compromise EPI’s performance,18,19 as well as to selectively ‘zoom’ into specific regions within tissues8,20 without suffering from folding artifacts.

The aim of the present study was to explore the possibility of relying on SPEN’s spatially-progressive excitation scheme, also to correct for B_1 inhomogeneities across the volume of interest. Non-uniform B_1‘s are an intrinsic characteristic of many MRI setups, particularly those associated with surface coils.21 Although the detection profile associated to such non-uniform B_1’s can be corrected using post-acquisition image processing,34 they do not compensate for losses in SNR. This is by contrast to adjustments in the RF excitation profile, which if performed during the application of the pulse can make up for lost signal intensities. Several methods have been developed to achieve this, including the use of complex RF pulses that incorporate the B_1 profile in addition to the required slice

selection24,25, multi-channel transmit arrays allowing RF transmit control26,27, and adiabatic RF pulses28, 29. The latter are relatively easy to implement and do not require specialized hardware, but when incorporated into ultrafast imaging sequences such as EPI, require long echo times that lead in turn to a need for using multiple, segmented acquisitions.30 As is shown here, modulating the pulse amplitude of SPEN's "chirped" encoding pulse along the main direction of the B_1 field inhomogeneity, allows one to compensate for the RF inhomogeneity and thus improve image fidelity and sensitivity. A particularly simple way of finding a suitable modulation is here demonstrated in both phantom and *in vivo* experiments using surface coils, where the performances of SPEN sequences that employ this compensation are compared against EPI experiments.

2 Exploiting SPEN's spatial encoding for compensating B_1^+ inhomogeneities

SPEN's encoding (Figure 1) is usually implemented using a chirped pulse combined with an excitation gradient, imparting a parabolic phase to be decoded during the acquisition. If implemented in a so-called "hybrid" single-shot 2D mode, this spatial encoding acts along the low-bandwidth direction (assumed here to lie along y and to extend over a field of view FOV), while a regular k-space encoding acts along the readout direction (taken along x). The chirped pulse waveform executing SPEN's excitation/encoding can be expressed as

$$RF(t)=B_1(t)e^{i\varphi_1(t)} \quad (1)$$

where $B_1(t)$ defines an envelop that here will usually be a WURST-40 shape $B_1(t) \propto (1 - \cos^{40}(\pi t/T_{enc}))$,31 T_{enc} is the pulse duration, and $\varphi_1(t) = Rt^2/2 + O_i t$ defines the rotating-frame phase of a linear frequency sweep, whose rate is $R = BW/T_{enc}$ and bandwidth is BW = $-2O_i = \gamma G_{enc} FOV$. The action of this chirped RF takes place while under the application of a gradient G_{enc}; following the encoding and an eventual spin-echo pulse, the signal is then collected over a time T_{acq} while under the action of an acquisition gradient G_{acq}. For simplicity we shall also assume that the B_1 inhomogeneity caused by the surface coil is one-dimensional, and that its main axis also coincides with the y-sweep direction. Under the usual assumption that the chirped pulse excites each of the spin packets progressively along their y location, one can elaborate a signal expression to include potential $M_+(y)$ heterogeneities in the excited magnetization profile as well as potential $C(y)$ receiver inhomogeneities:

$$S(t) \propto \int_{-\frac{FOV}{2}}^{\frac{FOV}{2}} C(y)M_+(y)\rho(y)e^{i(\varphi_{enc}(y)+k(t)y)}dy \quad (2)$$

Here $\varphi_{enc}(y) \propto y^2$ is the parabolic phase imparted by the chirped encoding pulse,13 $k(t)=\gamma\int_0^t G_{acq}(t')dt'$ is the wavenumber accrued as a function of the acquisition time t, and $\rho(y)$ is the spin density being sought. In past SPEN analyses we had assumed uniform

transmit and receive RF profiles, and thereby to $C(y)M_+(y) = 1$. In the present instance, however, we describe the dependencies in the RF transmit and receive profiles as

$$C(y)M_+(y) \propto B_1^-(\mathrm{y}) \sin\left(B_1^+(y)\right). \quad (3)$$

Here $B_1^+(y)$ is the profile of the RF pulse imparting its effects on $M_+(y)$ via the sine of the excitation angle, and $B_1^-(y)$ is the receiving field sensitivity associated to the acquisition. 32,33

Equation (3) suggests that upon employing surface or other inhomogeneous coils, two attenuation/distortion sources arise: one related to the RF transmission, and the other to the reception. Since the receiving profile distortions can be compensated to some extent by post-processing,34 we focus on correcting the transmission as main goal of this study. To do so we rely again on the stationary phase approximation,13 which for a relaxation-free scenario predicts that the signal $S(t)$ at each time point will be proportional to the local spin magnetization and density, according to $S(t) \propto \sin\left(B_1^+(y_0(t))\right) \rho(y_0(t))$ –with y_o the coordinate fulfilling $\left[\frac{\partial \varphi_{enc}[y(t)]}{\partial y}\right]_{y=y_0} = 0.$ Therefore, if one would modify the encoding pulse WURST envelop $B_1(t)$ with a modulation that *a priori* guarantees that $sin(B_1^+(y_0(t)))=1$, the resulting excitation inhomogeneities should be minimized. Figure 1c illustrates an example of such a RF-based profile correction, based on a simplified B_1-heterogeneity model. Naturally, there is a limit to the kind of B_1-derived corrections one can apply: eventually the RF power required for the compensation would exceed the capabilities of the scanner, of the coil, or of the power that one is allowed to deposit on the subject.

To implement the correction just described, it is necessary to measure the actual B_1 profile and utilize this information in the design of the RF chirp pulse. Numerous methods have been proposed for quantitatively measuring the spatial dependence of a B_1;18, 19 however, since in our case it is only the *relative* variation of the profile along the *y*-axis *with* B_1 that is actually required, a simpler alternative consists of measuring the spatial projections $I(y)=\int_{X-axis}\rho(x,y)dx$ afforded by an array of single-shot 2D SPEN acquisitions, repeated as a function of excitation power. This can be carried out efficiently and with good robustness vis-à-vis B_0 inhomogeneity. Such set of measurements (Figures 2-I, 2-II) can then be translated into maps of the optimum B_1 intensities that should be used –in Gauss, kHz, arbitrary db settings, or other units on which the scanner relies for its RF power handling– versus position *y*. Translating *y*-positions into *t*-excitation times as $y = -FOV/2 + FOV\cdot(t/T_{acq})$, yields then the *t*-dependent RF amplitude by which the original profile should be corrected for in order to retrieve an optimal image (Figures 2-III, 2-IV). A point to consider in such procedure is the nature of y_o, which can in principle be start at $\pm FOV/2$. When using the scheme in Figure 1, it is convenient to choose the initial y_o – which being the first point to be excited and last one to be detected will be the position most strongly affected by T_2 losses– as the position closest to the surface coil; in Fig. 2 this position would correspond to +FOV/2. SPEN-like sequences that are devoid of spatially-dependent T_2

Europe PMC Funders Author Manuscripts

effects like RASER,20 or SPEN sequences relying on a swept 180° pulse for the encoding, 35,36 would be exempt from such need. Still, a similar procedure as the one just described would deliver the *y*-independent, maximum sensitivity profiles also for such alternative encoding schemes.

3 Experimental

MR measurements

In vitro and *in vivo* measurements were performed on a 9.4 T/ 31 cm actively shielded animal scanner (Magnex Scientific, Oxford, UK) equipped with a 12-cm-inner-diameter gradient (400 mT/m in x,y,z directions; Magnex Scientific) and interfaced to a VNMRS® console (Varian Inc., Palo Alto CA, USA). A custom-designed quadrature ^{1}H surface coil consisting of two geometrically decoupled 16-mm diameter single loops, was used as transmitter/receiver probe. B_o field inhomogeneity was corrected using the FASTMAP protocol38. *In vitro* tests were carried out on tap water phantoms. *In vivo* measurements were performed on male Sprague-Dawley rats with 350 gr average weights; the animals were anesthetized using 1.5% isoflurane and their physiology was monitored throughout the scans. All experiments were approved by the local ethics committee.

Pulse sequences and processing

SPEN acquisitions were implemented using the sequence in Figure 1a, with RF pulses and gradient shapes designed in Matlab® (The MathWorks Inc., Natick, MA) and uploaded onto the scanner. The SPEN image reconstruction was also performed using custom-written Matlab packages, which included a super-resolution (SR) processing of the data along the spatiotemporal dimension, 37 and a conventional FT along the *k*-dimension. Pre-SR data manipulations included minor realignments of positive and negative readout echoes. The SPEN images were compared against SE EPI measurements performed using pulse sequences provided with the Varian scanner. For the single-shot EPI tests these used a 90° sinc pulse for slice selection and a slice-selective 180° pulse for refocusing. Interleaved four-shot SE-EPI experiments were also done,30 using pairs of adiabatic hyperbolic secant pulses for the echoing. For the DWI measurement comparisons, pulsed field gradients were placed symmetrically around the 180° refocusing inversion pulses in both SE-EPI and SPEN acquisitions. The diffusion weighing in the SPEN acquisitions was estimated taking into consideration the *b*-values dependence along the y-direction, as described in Ref. 14.

To evaluate the B_1 profiles and implement the corrections described in Figure 2, a series of constant-RF-amplitude acquisitions based on WURST-40 pulse shapes was performed, while varying the maximum pulse power over 19 equally-stepped B_1 db-values. These single-scan experiments placed the spatiotemporally encoded dimension along the main inhomogeneity axis of the B_1 field. The final 1D power profile to be applied in B_1-compensated experiments was obtained by extracting for each location the B_1 that delivered maximal signal intensity, making a composite of these maximum-intensity $B_1(y(t))$ values, and then smoothing the ensuing waveform profile (Figure 2-IV). Bloch-equation simulations (Figure 1d) confirmed the accuracy of this procedure. This correction method was adopted for both *in vitro* and *in vivo* measurements.

4 Results

Phantom experiments

Figure 3 compares spin echo SPEN images acquired on a water phantom sample, with and without the B_1-compensation procedure just described. Panel (a) illustrates how, due to the coil's inhomogeneity, increasing the maximum amplitude of the chirped pulse used to impart the SPEN, enables one to highlight progressively deeper regions along the *y*-axis, as they depart from the position of the surface coil. Average $I(y,B_1)$ plots (Fig. 3b) yield the RF settings that should be used for optimizing the amplitudes as a function of *y*/*t*; the improvements brought about by the correction in terms of spatial homogeneity and signal intensity are evidenced by the 2D image shown in Figure 3c. As also shown in this panel, changing the maximum RF power will then scale the overall signal intensity, but will no longer introduce appreciable distortions as a function of depth. This is further illustrated in Fig. 3d, which depicts the intensity profiles *I* that are then observed versus power and y direction. Finally, Figure 3e highlights the improved spatial coverage that can be obtained by this B_1 correction mode.

In vivo measurements

The performance of this B_1-correction approach was also evaluated in single-scan *in vivo* acquisitions. SE-EPI images were acquired and compared to SPEN acquisitions collected with and without the B_1 compensation algorithm, using two different approaches. One included a single-shot, regular SE-EPI sequence; the other utilized a SE-EPI incorporating two 180° adiabatic refocusing pulses for enhancing the robustness vis-à-vis B_1 inhomogeneities. These data, shown in Figure 4, evidences once again a clear improvement in FOV coverage along the main axis of the surface coil (Figs. 4d and 4g); this improvement results in both a higher signal sensitivity, as well as the higher fidelity that SPEN images usually display vis-à-vis EPI counterparts. As for the different contrasts evidenced by the SPEN and EPI images, these are most likely owing to the different T_2 weightings of the two experiments.13

One of the promising applications of SPEN is DWI –particularly at high fields or in heterogeneous tissues liable to susceptibility distortions14,39,40. To explore the potential improvements that the B_1-corrected SPEN scheme hereby introduced could bring to DWI, single scan experiments were acquired on a rat brain with the same surface coil setup as in Figure 4, for different b-values. These images were compared to comparable data arising from single-scan diffusion-weighted SE-EPI experiments. As once again evidenced in Figure 5, larger FOVs along the *y*-direction endowed with better sensitivity, could be achieved thanks to the enhanced coverage of the corrected SPEN procedure. Calculated apparent diffusion coefficient (ADC) maps obtained from both schemes were nevertheless similar in regions where quality signals were available; this evidences another potential advantage of SPEN for this kind of DWI investigations.

5 Discussion and Conclusions

The present study explored a simple approach to correct for uniaxial RF inhomogeneity distortions, of the kind that normally will arise upon operating with a single transmit/receive surface coil. It was shown that high-SNR and high-fidelity single-shot MR images can then be acquired, by exploiting the coaxiality between the distortions introduced by an uneven B_1 excitation, and the spatiotemporal encoding process executed by a frequency-swept chirp pulse. By performing a rapid series of SPEN calibration measurements based on scans as a function of B_1 value, power levels capable of offsetting the dropping B_1s associated to the use of a surface coil could be found. When considering the kind of distortions associated to the use of surface coils, which are liable to be load-dependent and hence in need of precalibrations for different samples, the present method is particularly convenient. Incorporating such predetermined B_1s into a revised chirped excitation profile extended the achievable FOV coverage and increased the overall signal, in a relatively simple fashion. These improvements were evidenced by both *in vitro* and *in vivo* tests, including a 2D diffusion-weighted imaging study of a rat brain that demanded a single 27 ms chirp pulse with only 130 mW of mean RF power –well suited to a majority of surface coil assemblies. The ensuing spatial coverage and sensitivity of the SPEN-derived ADC maps, compared then favorably with those arising from the EPI images. This not only resulted from the new B_1 correcting procedure, but also from SPEN's already-reported robustness to B_0 inhomogeneities.

The present study focused on a particularly simple geometrical distortion of the B_1 profile, which could then be compensated by a particularly simple and rapid calibration/correction procedure. More complex procedures and extensions to alternative geometries, could naturally be conceived. In terms of surface coil distortions, which are liable to be load-dependent and hence in need of precalibrations for different samples, the present method is particularly convenient. Alternatives could include making an actual map of the nutation frequencies in a two-dimensional plane, and derive the corrections to be performed from there. Indeed, although in the present work the B_1 correction was performed along a single axis, the method can be extended to obtain planar compensation by implementing suitably adapted 2D spatiotemporal RF pulses41, 42. Such improvements might be unjustified in the simple surface-coil scenario hereby treated, yet Garwood *et al* have shown their worthiness in scenarios including high-field cases where the object being targeted is sited in inhomogeneous B_o and B_1 fields, which could then be simultaneously compensated by amplitude and phase manipulations of the chirped pulse.42 Yet another possibility could rest in departing from the use of a constant-rate chirp pulse, and tailor the rate of the sweep R to the actual strength of the B_1 value: as the spins' nutation angle is proportional to $B_1\sqrt{R}$, regions of weakening B_1s could be excited equally well by slower sweeps. Such procedures have indeed been demonstrated in SPEN acquisitions;12 their potential drawbacks include longer excitation times, and uneven spatial resolutions as a function of acquisition time. Alternatively VERSE-like approaches could be adopted43 whereby the G_{enc} gradient is reduced as a constant-rate chirp progresses, with similar advantages and drawbacks. Clearly, several interesting avenues arise in this area.

Europe PMC Funders Author Manuscripts

Acknowledgements

We are grateful to A. Seginer for helpful discussions and to A Capozzi and Y. Pilloud for their help in designing the hardware used for the MR measurements. This work was supported by ERC PoC Grant # 633888, the Israel Science Foundation ISF grant 795/13, the Kimmel Institute of Magnetic Resonance, the generosity of the Perlman Family foundation, the Swiss National Science Foundation (grant PP00P2_133562), the Centre d'Imagerie BioMédicale (CIBM) of the UNIL, UNIGE, HUG, CHUV, EPFL, the Leenards and Jeantet Foundations, and EU COST action TD1103.

Abbreviations

EPI	Echo-Planar Imaging
FOV	Field of View
MRI	Magnetic Resonance Imaging
RF	Radio frequency
SPEN	SPatiotemporal ENcoding
TE	Echo Time
TR	Repetition Time

References

1. Vinogradov E, Sherry AD, Lenkinski RE. CEST: from basic principles to applications, challenges and opportunities. J Magn Reson. 2013; 229:155–72. [PubMed: 23273841]
2. Van Zijl PC, Yadav NN. Chemical exchange saturation transfer (CEST): What is in a name and what isn't? Magn Reson Med. 2011; 65:927–48. [PubMed: 21337419]
3. Gallagher FA, Kettunen MI, Day SE, De-En Hu, Ardenkjær-Larsen J-H, Zandt R, Jensen PR, Karlsson M, Golman K, Lerche MH, Brindle KM. Magnetic resonance imaging of pH in vivo using hyperpolarized 13C-labelled bicarbonate. Nature. 2008; 453:940–943. [PubMed: 18509335]
4. Comment A, Merritt ME. Hyperpolarized Magnetic Resonance as a Sensitive Detector of Metabolic Function. Biochemistry. 2014; 53(47):7333–7357. [PubMed: 25369537]
5. Ogawa S, Lee TM, Kay AR, Tank DW. Brain magnetic resonance imaging with contrast dependent on blood oxygenation. Proc Natl Acad Sci. 1990; 87(24):9868–9872. [PubMed: 2124706]
6. LeBihan D, Breton E, Lallemand D, Grenier P, Cabanis E, Laval-Jeantet M. MR imaging of intravoxel incoherent motions: application to diffusion and perfusion in neurologic disorders. Radiology. 1986; 161:401–407. [PubMed: 3763909]
7. Basser PJ, Mattiello J, LeBihan D. MR diffusion tensor spectroscopy and imaging. Biophys J. 1994; 66(1):259–67. [PubMed: 8130344]
8. Haase A. Snapshot FLASH MRI. Applications to T1, T2 and Chemical-Shift Imaging. Magn Reson Med. 1990; 13:77–89. [PubMed: 2319937]
9. Hennig J, Nauerth A, Friedburg H. RARE imaging: A fast imaging method for clinical MR. Magn Reson Med. 1986; 3:823–833. [PubMed: 3821461]
10. Schmidt, F.; Stehling, MK.; Turner, R. Echo Planar Imaging: Theory, Technique and Application. Springer; Berlin: 1998.
11. Mansfield P. Multi-Planar Image Formation Using NMR Spin Echoes. J Phys C: Solid State Phys. 1977; 10:L55–58.
12. Shrot Y, Frydman L. Spatially-encoded NMR and the acquisition of 2D magnetic resonance images within a single scan. J Magn Reson. 2005; 172:179–190. [PubMed: 15649744]
13. Tal A, Frydman L. Single-scan multidimensional magnetic resonance. Prog Nucl Magn Reson Spectrosc. 2010; 57:241–292. [PubMed: 20667401]

14. Solomon E, Shemesh N, Frydman L. Diffusion weighted MRI by spatiotemporal encoding: Analytical description and in vivo validations. J Magn Reson. 2013; 232:76–86. [PubMed: 23562003]
15. Seginer A, Schmidt R, Leftin A, Solomon E, Frydman L. Referenceless Reconstruction of Spatiotemporally Encoded Imaging Data: Principles and Applications to Real-Time MRI. Magn Reson Med. 2014; 72:1687–1695. [PubMed: 24420445]
16. Goerke U, Garwood M, Ugurbil K. Functional magnetic resonance imaging using RASER. Neuroimage. 2011; 54(1):350–60. [PubMed: 20699123]
17. Tal A, Frydman L. Spectroscopic imaging from spatially-encoded single-scan multidimensional MRI data. J Magn Reson. 2007; 189:46–58. [PubMed: 17869559]
18. Tal A, Frydman L. Spatial encoding and the single-scan acquisition of high definition MR images in inhomogeneous fields. J Magn Reson. 2006; 181:179–194. [PubMed: 16843690]
19. Li J, Chen L, Cai S, Cai C, Zhong J, Chen Z. Imaging with referenceless distortion correction and flexible regions of interest using single-shot biaxial spatiotemporally encoded MRI. NeuroImage. 2015; 105:93–111. [PubMed: 25462700]
20. Chamberlain R, Park JY, Corum C, Yacoub E, Ugurbil K, Jack CR, Garwood M. RASER: a new ultrafast magnetic resonance imaging method. Magn Reson Med. 2007; 58(4):794–799. [PubMed: 17899612]
21. Axel L. Surface coil magnetic resonance imaging. J Comput Asist Tomogr. 1984; 8:381–384.
22. Vaughan JT, Garwood M, Collins CM, Liu W, Delabarre L, Adriany G, Andersen P, Merkle H, Goebel R, Smith MB, Ugurbil K. 7T vs. 4T: RF power, homogeneity, and signal-to-noise comparison in head images. Magn Reson Med. 2001; 46:24–30. [PubMed: 11443707]
23. Van de Moortele P-F, Akgun C, Adriany G, Moeller S, Ritter J, Collins CM, Smith MB, Vaughan JT, Ugurbil K. B_1 destructive interferences and spatial phase patterns at 7T with a head transceiver array coil. Magn Reson Med. 2005; 54:1503–1518. [PubMed: 16270333]
24. Saekho S, Boada FE, Noll DC, Stenger VA. Small tip angle three-dimensional tailored radiofrequency slab-select pulse for reduced b1 inhomogeneity at 3 T. Magn Reson Med. 2005; 53:479–484. [PubMed: 15678525]
25. Yip CY, Fessler JA, Douglas CN. Iterative RF pulse design for multidimensional, small-tip-angle selective excitation. Magn Reson Med. 2005; 54:908–917. [PubMed: 16155881]
26. Collins CM, Liu W, Swift J, Smith MB. Combination of optimized transmit arrays and some receive array reconstruction methods can yield homogeneous images at very high frequencies. Magn Reson Med. 2005; 54:1327–1332. [PubMed: 16270331]
27. Katscher U, Bornert P, Leussler C, van den Brink JS. Transmit SENSE. Magn Reson Med. 2003; 49:144–150. [PubMed: 12509830]
28. de Graaf RA, Luo Y, Terpstra M, Merkle H, Garwood M. A new localization method using an adiabatic pulse, BIR-4. J Magn Reson. 1995; 106(3):245–52.
29. Garwood M, Ugurbil K, Rath AR, Bendall MR, Ross BD, Mitchell SL, Merkle H. Magnetic Resonance Imaging with Adiabatic Pulses Using a Single Surface Coil for RF Transmission and Signal Detection. Magn Reson Med. 1989; 9:25–34. [PubMed: 2709994]
30. Van de Looij Y, Kunz N, Huppi P, Gruetter R, Sizonenko S. Diffusion tensor echo planar imaging using surface coil transceiver with a semiadiabatic RF pulse sequence at 14.1T. Magn Reson Med. 2011; 65:732–737. [PubMed: 20939068]
31. Kupce E, Freeman R. An adaptable NMR broadband decoupling scheme. Chem Phys Lett. 1996; 250:523–527.
32. Hoult DI. The principle of reciprocity in signal strength calculations - a mathematical guide. Concepts in Magn Reson. 2000; 4:173–187.
33. Collins CM, Smith MB. Signal-to-noise ratio and absorbed power as functions ofmain magnetic field strength, and definition of “90’ RF pulse for the head in the birdcage coil. Magn Reson Med. 2001; 45:684–691. [PubMed: 11283997]
34. Belaroussi B, Milles J, Carme S, Zhu YM, Benoit-Cattin H. Intensity non-uniformity correction in MRI: Existing methods and their validation. Med Image Anal. 2006; 10:234–246. [PubMed: 16307900]

35. Ben-Eliezer N, Frydman L. Spatiotemporal encoding as a robust basis for fast three-dimensional in vivo MRI. NMR Biomed. 2011; 24:1191–1201. [PubMed: 21360603]
36. Schmidt R, Frydman L. New Spatiotemporal Approaches for Fully-Refocused, Multi-Slice Ultrafast 3D MRI. Magn Reson Med. 2013; 71(2):711–722. [PubMed: 23468061]
37. Ben-Eliezer N, Irani M, Frydman L. Super-resolved spatially-encoded single-scan 2D MRI. Magn Reson Med. 2010; 63(6):1594–1600. [PubMed: 20512863]
38. Gruetter R, Tkac I. Field mapping without reference scan using asymmetric echo-planar techniques. Magn Reson Med. 2000; 43:319–323. [PubMed: 10680699]
39. Leftin A, Rosenberg JT, Solomon E, Bejarano F, Grant SC, Frydman L. Ultrafast in vivo diffusion imaging of stroke at 21.1T by spatiotemporal encoding. Magn Reson Med. 2015; 73:1483–1489. [PubMed: 24845125]
40. Solomon E, Nissan N, Furman-Haran E, Seginer A, Shapiro-Feinberg M, Degani H, Frydman L. Overcoming limitations in diffusion-weighted MRI of breast by spatio-temporal encoding. Magn Reson Med. 2015; doi: 10.1002/mrm.25344
41. Dumez J-N, Frydman L. Multidimensional excitation pulses based on spatiotemporal encoding concepts. J Magn Reson. 2013; 226:22–34. [PubMed: 23202845]
42. Snyder ALS, Corum CA, Moeller S, Powell NJ, Garwood M. MRI by steering resonance through space. Magn Reson Med. 2013; 72:49–58. [PubMed: 23913527]
43. Conolly S, Nishimura D, Macovski A, Glover G. Variable-rate selective excitation. J Magn Reson. 1988; 78:440–458.

Europe PMC Funders Author Manuscripts

Europe PMC Funders Author Manuscripts

Highlights

1. A method for compensating surface coil inhomogeneities in ultrafast MRI is presented
2. The method exploits the built-in heterogeneities of Spatiotemporal Encoding imaging sequences
3. Theoretical expectations were validated with 9.4 T MRI experiments on phantoms and *in vivo*

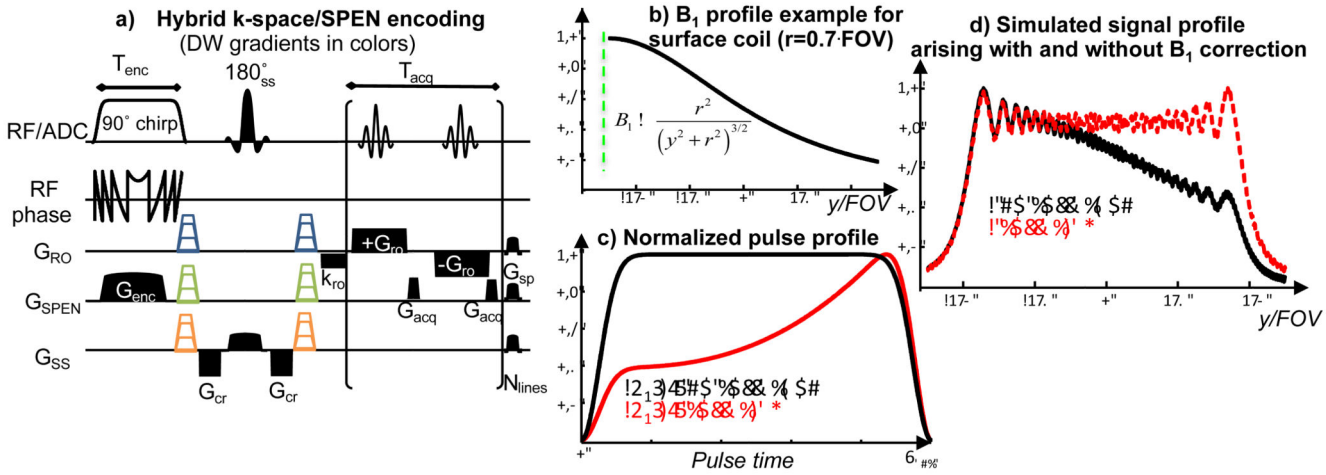

Figure 1.

(a) Single-shot Hybrid 2D SPEN sequence based on a 90˚ chirp encoding and spin echo. G_{SS}, G_{enc}, G_{ro}, G_{acq}, G_{cr}, G_{sp}: slice-selective, SPEN encoding, *k*-readout, SPEN decoding, crusher and spoiling gradients, respectively. Shown in colors are stepped diffusion-weighting blocks applied along all directions for a DWI scan. (b) B_1 profile characteristic of a surface coil of radius *r*, with the dashed green line denoting the coil's position. (c) Amplitude correction to be imparted by the algorithm presented in this work to a WURST-like chirped pulse, to achieve compensation of the B_1^+irradiation RF during the SPEN encoding process. (d) Signal profiles predicted by a Bloch simulation, with and without B_1^+ compensation for the RF inhomogeneity depicted in panel (c).

Europe PMC Funders Author Manuscripts

Europe PMC Funders Author Manuscripts

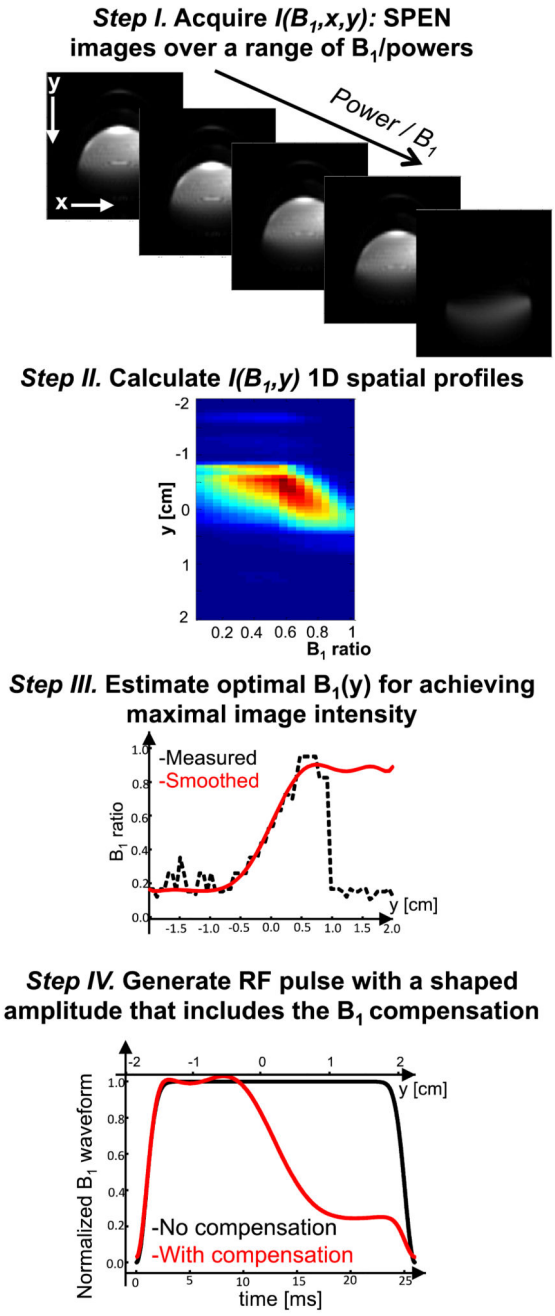

Figure 2.

Procedure used for correcting uniaxial B_1 inhomogeneities in SPEN images. Step I: a series of single-shot SPEN images are acquired over an array of RF power values. Step II: images are projected to obtain 1D spatial profiles *vs* normalized B_1 RF power. Step III: these $I(B_1,y)$ profiles are used to extract optimal B_1 powers providing maximal image intensity at each position y. Step IV: after suitable smoothing, the $B_1(y)$ dependence is translated into time over the course of the encoding according to $t = T_{acq}\,(y/FOV+0.5)$, to obtain the final $B_1(t)$ amplitude modulation. Results in this experimental example involved the sequence in Fig. 1a

with the following main acquisition parameters: FOV of 4x4 cm^2 for single slice of 2 cm thickness, acquisition dwell time 4 us, T_{enc} = 27 ms, G_{enc} = 0.6 G/cm, T_{acq} = 27 ms, 64 x 64 matrix size with in-plane resolution of 0.6 x 0.6 mm^2.

Europe PMC Funders Author Manuscripts

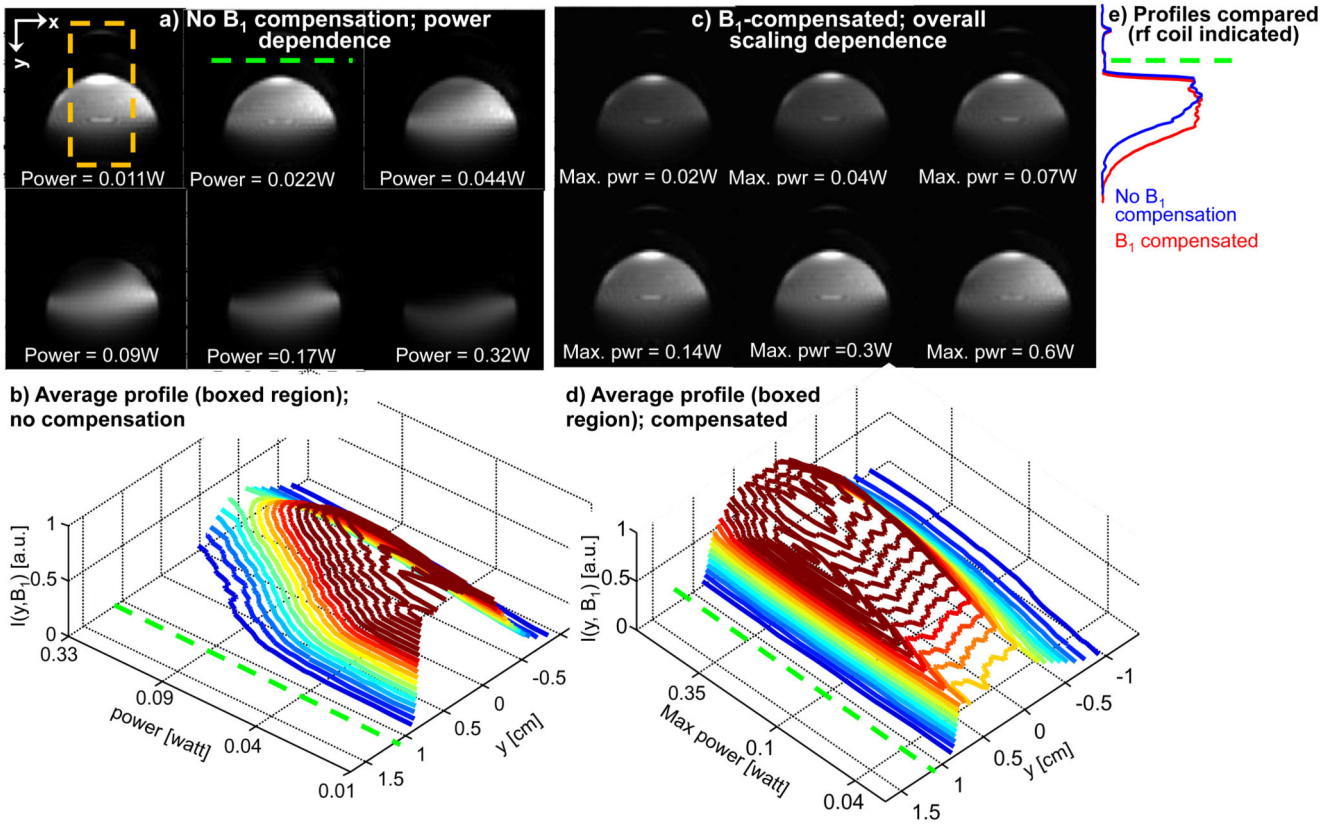

Figure 3.

SPEN images acquired on a phantom filled with water, while varying the RF amplitude of the encoding chirped pulse without (a,b) and with (c,d) B_1 compensation. Image profiles $I(y,B_1)$ are visualized as profiles in (b) and (d) by averaging the 2D spatial maps in (a) and (c), over the area delimited by the yellow square. B_1 compensation proceeded by suitable waveforming of the pulse, as described in Figure 2. Maximal intensity profiles $I_{max}(y)$ without and with B_1^+ compensation are displayed in (e), obtained for the power yielding the highest overall SNR SPEN image (corresponding to a 33 dB setting; ~230 mW of maximum RF power). Indicated by the dashed green line is the approximate position of the surface coil used in these scans.

Europe PMC Funders Author Manuscripts

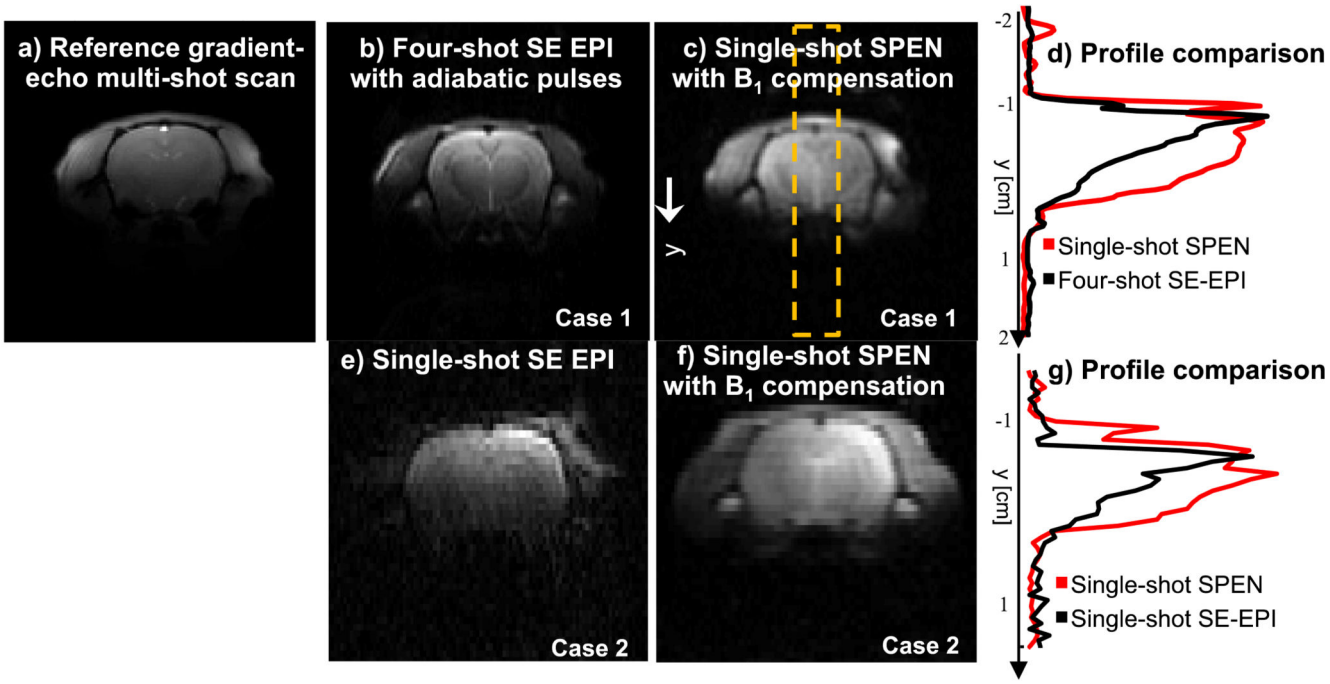

Figure 4.

EPI and SPEN comparisons between *in vivo* rat brain images acquired on two different animals. (a-c) Multi-shot gradient-echo, four-shot interleaved SE-EPI and B_1-corrected SPEN images, respectively; shown for completion in (d) are *y*-axis profiles across the indicated dashed yellow box. (e-g) Idem but involving single-shot experiments. SPEN acquisition parameters were as detailed in Fig. 2. Single-shot SE-EPI parameters were: dwell time 4 μs, T_{acq} = 23 ms, TE = 31 ms, 128 x 64 matrix size (in-plane resolution of 0.3 x 0.6 mm^2), no adiabatic pulses. Four-shot SE-EPI parameters were: twice refocused echoing with hyperbolic secant adiabatic pulses (bandwith = 6.4 kHz, duration = 2.5 ms), dwell time = 5.2 μs, T_{acq} = 16 ms, TE = 43 ms, 128 x 64 acquired points (resolution of 0.3 x 0.6 mm^2). Gradient echo reference scan parameters were: TE = 3 ms, TR = 6ms, 128 x 128 matrix size.

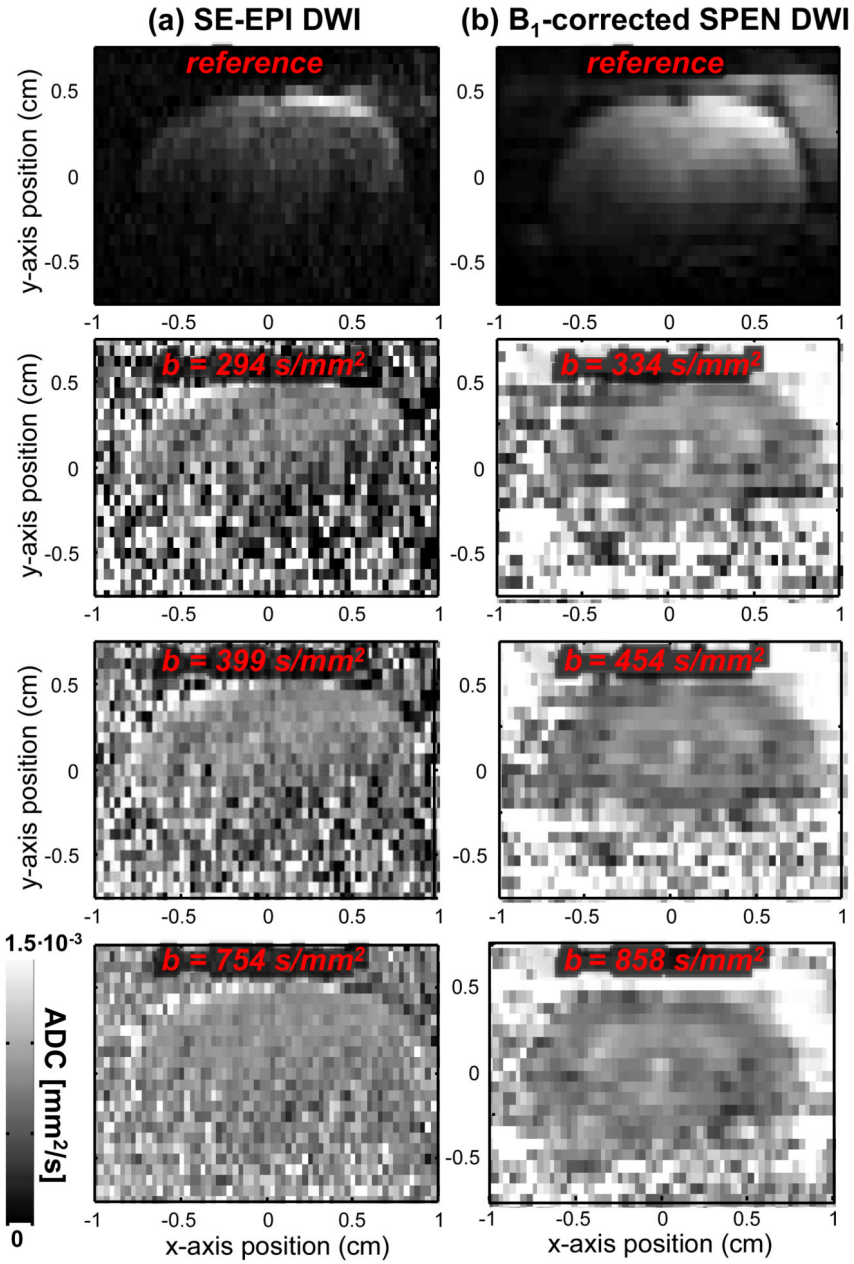

and Δ = 16.9 ms in SPEN.

Figure 5.

ADC maps collected on a healthy rat brain acquired using single-scan SE-EPI (left column) and B_1-corrected SPEN (right column) sequences, together with their corresponding $b = 0$ reference scans (top). The *b*-values indicated on top of each ADC map denote the average range of b's used in the maps' derivations; three sets of measurements (with diffusion-sensitizing gradients along orthogonal directions) were made to compute these isotropic ADC maps. SPEN acquisition parameters were as those presented in Figure 2, apart for the inclusion of the diffusion gradients (and their delays). SE-EPI parameters were: Dwell time

4 us, T_{acq} = 32 ms, TE = 58.67 ms, 128 x 64 matrix size (in-plane resolution of 0.3 x 0.6 mm^2). Diffusion parameters δ = 3 ms gradient pulses for all sequences, intergradient delay Δ = 20 ms in SE-EPI and Δ = 16.9 ms in SPEN.

Europe PMC Funders Author Manuscripts